Semiclassical analysis of a two-electron quantum dot in a magnetic field: Dimensional phenomena

R. G. Nazmitdinov

Max-Planck-Institut für Physik Komplexer Systeme, D-01187 Dresden, Germany
and Bogoliubov Laboratory of Theoretical Physics, Joint Institute for Nuclear Research, 141980 Dubna, Russia

N. S. Simonović and Jan M. Rost

Max-Planck-Institut für Physik Komplexer Systeme, D-01187 Dresden, Germany

It is shown that with the inclusion of the vertical extension of a quantum dot the experimental findings of Ashoori *et al.* [Phys. Rev. Lett. **71**, 613 (1993)] can be modeled consistently with a parabolic confinement. Furthermore, the magnetic properties such as the magnetic moment and the susceptibility are sensitive to the presence and strength of a vertical confinement. Using a semiclassical approach the calculation of the eigenvalues reduces to simple quadratures providing a transparent and almost analytical quantization of the three-dimensional quantum dot energy levels that differ from the exact energies only by a few percent. While the dynamics for three-dimensional axially symmetric two-electron quantum dot with parabolic confinement potentials is in general nonseparable due to the Coulomb interaction we have found an exact separability for specific values of the magnetic field.

I. INTRODUCTION

Current nanofabrication technology allows one to control the size and shape of quantum dots.[1–3] Due to the confinement of the electrons in all three spatial directions the energy spectrum is quantized creating excellent experimental and theoretical opportunities to study *controlled* single-particle and collective dynamics at the atomic scale. Depending on the experimental setup, the spectrum of a quantum dot displays shell structure[4–6] or follows predictions of random matrix theory (for a review see, Ref. 7). Furthermore, it becomes possible to trace the transition from a quantum mechanical to an almost classical regime.

Few-electron quantum dots have attracted special attention,[4,8] since they may provide a natural realization of a quantum bit.[1] The simplest quantum dot (QD) with the essential features of more complex systems contains two electrons. Experimental data, including transport measurements[9,10] and spin oscillations in the ground state under a perpendicular magnetic field[11–13] in two-electron QD's, have been explained quantum mechanically as a result of the interplay between the two-dimensional (2D) lateral confinement potential, electron correlations, and the magnetic field.[14–17] However, the usual 2D interpretation of the experiments[10,11] leads to inconsistencies[10,17] that can be avoided if one takes into account the 3D physical nature of the QD, as we will show in the following.

We will investigate these dimensional effects semiclassically that makes almost analytical solutions possible. Hence, we are able to trace the dynamical effects of the confinement strength, the magnetic-field strength, the Coulomb repulsion, and their mutual interplay in a way complementary to the full numerical approaches. In particular, the possibility for full separable dynamics despite the interaction of the electrons is clearly visible in the classical dynamics for certain values of the magnetic field. However, in contrast to a circular (2D) two-electron QD whose classical dynamics is al-

ways separable and, therefore, regular, the corresponding 3D system with axial symmetry is in general a nonintegrable problem with typical features of mixed dynamics (regular/chaotic). In Sec. II we briefly discuss this classical dynamics of the relative two-electron motion in a QD. The semiclassical quantization including an adiabatic approximation follows in Sec. III. We discuss the results and the consequences for the interpretation of the respective experiments in Sec. IV. The paper ends with a summary given in Sec. V.

II. THE MODEL AND CLASSICAL DYNAMICS

The Hamiltonian for the 3D two-electron QD reads

$$
H = \sum_{j=1}^{2} \left\{ \frac{1}{2m^*} \left(\mathbf{p}_j - \frac{e}{c} \mathbf{A}_j \right)^2 + \frac{m^*}{2} [\omega_0^2(x_j^2 + y_j^2) + \omega_z^2 z_j^2] \right\},
$$
$$
+ V_C + H_{\text{spin}}, \tag{1}
$$

where $V_C = \alpha / |\mathbf{r}_1 - \mathbf{r}_2|$ is the Coulomb energy [$\alpha = e^2/(4\pi\varepsilon\varepsilon_0)$] and $H_{\text{spin}} = g^* \mu_B (\mathbf{s}_1 + \mathbf{s}_2) \cdot \mathbf{B}$ describes the Zeeman energy, where $\mu_B = e\hbar/2m_e c$ is the Bohr magneton. Here m^* and g^* are the effective electron mass and g factor, respectively, and ε is the dielectric constant. The confining potential is approximated with a 3D axially symmetric harmonic oscillator and $\hbar\omega_z \neq \hbar\omega_0$ are the energy scales of confinement in the z direction and in the (x, y) plane, respectively. For the typical voltage ~ 1 V applied to the gate, the confining potential is some eV deep that is large compared to the few meV of the confining frequency.[2,3] Hence, the electron wave function is localized close to the minimum of the well that always can be approximated by a parabolic potential. In real samples the electron-electron interaction is usually screened. However, the pure Coulomb interaction should suffice to understand the main features of the system. For the perpendicular magnetic field ($\mathbf{B} \| z$) we choose a gauge described by the vector $\mathbf{A} = [\mathbf{B} \times \mathbf{r}]/2 = \frac{1}{2}B(-y, x, 0)$. Introduc-

ing the relative and center-of-mass coordinates $\mathbf{r} = \mathbf{r}_1 - \mathbf{r}_2$, $\mathbf{R} = \frac{1}{2}(\mathbf{r}_1 + \mathbf{r}_2)$, the Hamiltonian, Eq. (1), can be separated into the center of mass (CM) H_{CM} and relative motion H_{rel} terms: $H = H_{CM} + H_{rel} + H_{spin}$. The solution to the CM Hamiltonian is well known[18] and the effect of the Zeeman energy has been discussed in Refs. 14 and 15. In the following we will concentrate on the dynamics of H_{rel}.

For our analysis it is convenient to use cylindrical *scaled* coordinates, $\tilde{\rho} = \rho/l_0$, $\tilde{p}_\rho = p_\rho l_0/\hbar$, $\tilde{z} = z/l_0$, $\tilde{p}_z = p_z l_0/\hbar$, where $l_0 = (\hbar/\mu\omega_0)^{1/2}$ is the characteristic length of the confinement potential with the reduced mass $\mu = m^*/2$. The strength parameter α of the Coulomb repulsion goes over to $\lambda = 2\alpha/(\hbar\omega_0 l_0)$. Using the effective mass $m^* = 0.067 m_e$, the dielectric constant $\varepsilon = 12$, which are typical for GaAs, and the confining frequency $\hbar\omega_0 = 3$ meV, we obtain $\lambda \approx 3$. Hereafter, for the sake of simplicity, we drop the tilde, i.e., for the scaled variables we use the same symbols as before scaling.

In these variables the Hamiltonian for the relative motion takes a particular simple form (in units of $\hbar\omega_0$)

$$\epsilon \equiv \frac{H_{rel}}{\hbar\omega_0} = \frac{1}{2}\left[p_\rho^2 + \frac{m^2}{\rho^2} + p_z^2 + \left(\frac{\omega_\rho}{\omega_0}\right)^2 \rho^2 + \left(\frac{\omega_z}{\omega_0}\right)^2 z^2 \right.$$

$$\left. + \frac{\lambda}{\sqrt{\rho^2 + z^2}} \right] - \frac{\omega_L}{\omega_0} m, \qquad (2)$$

where $m = l_z/\hbar$, $\omega_L = eB/2m^*c$ is the Larmor frequency and

$$\omega_\rho = (\omega_L^2 + \omega_0^2)^{1/2} \qquad (3)$$

is the effective confinement frequency in the ρ coordinate that depends through ω_L on the magnetic field.

Due to the cylindrical symmetry, the z component $l_z \equiv p_\phi$ of the angular momentum is conserved and the motion in ϕ is separated from the motion in the (ρ, z) plane. Since the Coulomb term couples the two coordinates, the problem is in general nonintegrable that is reflected in the Poincaré sections shown in Fig. 1 for increasing magnetic field. The chosen ratio $\omega_z/\omega_0 = 3$ is of the same order of magnitude as in the experiment.[19] For $\omega_L = 0$ and small values of m the motion is mainly chaotic [see Fig. 1(a)]. With the magnetic field the frequency of oscillations along the ρ coordinate can be controlled that leads to qualitatively different dynamical situations [Figs. 1(b)–1(d)]. For equal effective confinement frequencies $\omega_\rho^2 = \omega_z^2$, the Hamiltonian Eq. (2) becomes separable in spherical coordinates and the dynamics is integrable [Fig. 1(c)]. For two other limiting cases, the dynamics is nearly integrable, namely, in the limit $m \to \infty$ and for $\omega_z \to \infty$. The latter case represents a two-dimensional QD, classically, we have $p_z, z \to 0$ in this limit.

III. SEMICLASSICAL QUANTIZATION AND CLASSICAL ADIABATIC TREATMENT

We will use a one-dimensional WKB-type quantization that allows us to reduce the dynamical problem to quadratures. This is possible since we can effectively separate the dynamics in all degrees of freedom (see below), either due to
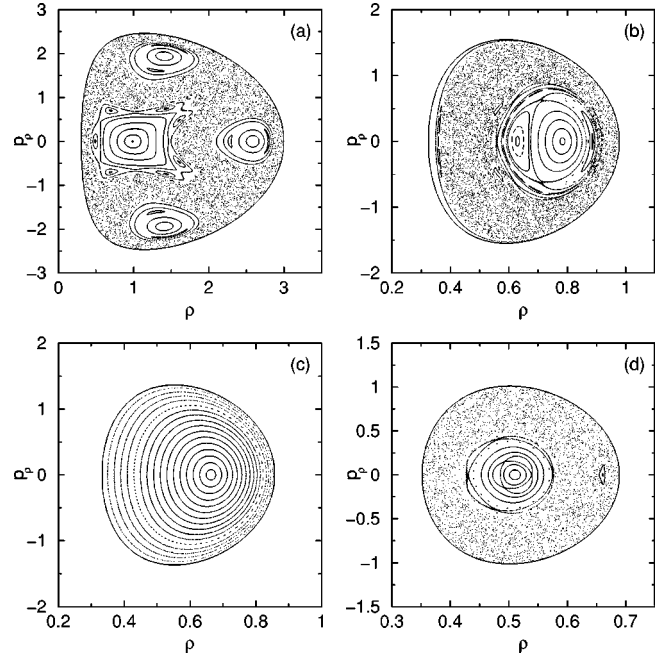

FIG. 1. Poincaré surfaces of sections $z = 0$, $p_z > 0$ of the relative motion for the axially symmetric 3D two-electron quantum dot ($\omega_z/\omega_0 = 3, \lambda = 3, m = 0, \epsilon = 5$) in the magnetic field for: (a) $\omega_L = 0$, (b) $\omega_L/\omega_0 = 2.5$, (c) $\omega_L/\omega_0 = \sqrt{8}$, and (d) $\omega_L/\omega_0 = 3.3$. The section (c) indicates that for the corresponding value of the magnetic field the system is integrable.

exact symmetries or due to different time scales that allow us to apply a classical adiabatic approximation in terms of the "removal of resonances" method (RRM). The RRM is widely used in classical problems of nonlinear dynamics and in celestial mechanics.[20]

A. Integrable cases

1. The circular 2D quantum dot

The semiclassical quantization of the circular 2D quantum dot is particularly simple since it reduces to a one-dimensional WKB quantization of the ρ motion due to the separability of the problem. For given m and $p_z = z = 0$ the momentum p_ρ determined from Eq. (2) enters the action integral

$$I_\rho = \frac{\hbar}{2\pi} \oint p_\rho \, d\rho = \frac{\hbar}{\pi} \int_{\rho_{min}}^{\rho_{max}} |p_\rho| \, d\rho, \qquad (4)$$

with the turning points ρ_{min}, ρ_{max} as the positive roots of equation $p_\rho(\rho) = 0$. The WKB quantization conditions

$$I_\rho(\epsilon) = \hbar\left(n_\rho + \frac{1}{2}\right), \quad n_\rho = 0, 1, \ldots, \quad m = 0, \pm 1, \ldots \qquad (5)$$

determine the energy levels. For noninteracting electrons ($\lambda = 0$) the analytical calculation of the action integral [see Eq. (A7)] leads to the (quantum mechanically exact) eigenenergies
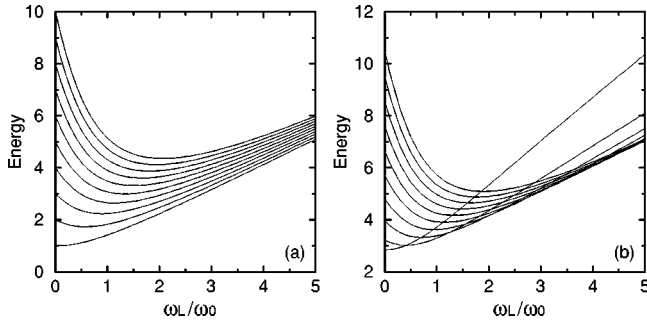
FIG. 2. The energy spectrum of the circular 2D quantum dot (in units $\hbar\omega_0$) as a function of the ratio ω_L/ω_0 for $n_\rho=0$ and $m=0,\ldots,9$ in the cases: (a) $\lambda=0$ and (b) $\lambda=3$.

$$\epsilon=\sqrt{1+\left(\frac{\omega_L}{\omega_0}\right)^2}(2n_\rho+|m|+1)-\frac{\omega_L}{\omega_0}m, \qquad (6)$$

which are the well-known Fock-Darwin energies.[18] For $\lambda \neq 0$, we calculate the action integral Eq. (4) numerically with a few iterations to determine the quantum eigenvalues. The energy spectra for noninteracting and interacting electrons are shown in Fig. 2. In the interacting case the semiclassical result, although not exact (the error is less than 1%), reproduces very well the quantum-mechanical results.[14,15]

2. Separability for the 3D quantum dot

Turning now to the 3D quantum dot we have seen that the dynamics is separable for $\omega_z^2=\omega_\rho^2\equiv\omega_L^{*2}+\omega_0^2$ and the Hamiltonian Eq. (2) in scaled spherical coordinates takes the form

$$\epsilon=\frac{1}{2}\left\{p_r^2+\left(\frac{\omega_z}{\omega_0}\right)^2r^2+\frac{\lambda}{r}+\frac{(l/\hbar)^2}{r^2}\right\}-\frac{\omega_L^*}{\omega_0}m. \qquad (7)$$

In this case the square of the total angular momentum $\mathbf{l}^2$ is an additional integral of motion. Therefore, the classical dynamics reduces again to a one-dimensional, radial problem. Using Eq. (7) and calculating the action integral for the radial motion analogous to that in Eq. (4) (i.e., with r instead of ρ), we obtain the energy levels from the standard WKB quantization conditions

$$I_r(\epsilon)=\hbar\left(n_r+\frac{1}{2}\right), \quad |\mathbf{l}|=\hbar\left(l+\frac{1}{2}\right),$$

$$n_r,l=0,1,\ldots, \quad m=0,\pm 1,\ldots,\pm l. \qquad (8)$$

Note that it is only the magnetic field that generates the spherical symmetry of the problem and, therefore, its separability leading to three good quantum numbers n_r, l, and m.

The restoration of the rotational symmetry of the electronic states by the magnetic field for noninteracting electrons is a well-known fact (see, for example, Refs. 6,21). This phenomenon was also recognized in the results for *interacting* electrons in self-assembled QD's.[22] It was interpreted in Ref. 22 as an approximate symmetry that had survived from the noninteracting case due to the dominance of the confinement energy over the relatively small Coulomb interaction energy. However, as it is clear from the form of Eq. (7), the symmetry is not approximate but *exact* even for strongly interacting electrons because the radial electron-electron repulsion does not break the rotational symmetry.

B. Adiabatic approximation for the 3D quantum dot

In the general case ($\omega_\rho\neq\omega_z$) of an axially symmetric 3D quantum dot we have nonintegrable motion and a semiclassical quantization is neither straightforward nor does it give results that allow for a simple understanding of the dynamics. For the parameters we have chosen the contribution of the Coulomb interaction to the total energy is comparable to the confinement energy at zero magnetic field and it becomes for small m even more important with increasing magnetic field [compare Figs. 2(a) and 2(b)]. In this case, the standard perturbation theory is not valid, since the Coulomb interaction prevails over the confinement energy. Therefore, we make use of the fact that in real samples the confining potential in the z direction is much stronger than in the (x,y) plane that allows us to analyze the 3D nonintegrable system with the RRM. To lowest order the RRM consists of averaging the Hamiltonian function over the fastest angle of the unperturbed motion ($\lambda=0$) after rewriting coordinates and momenta in terms of action-angle variables $(J_\rho,J_z,\theta_\rho,\theta_z)$. The original coordinates of the 3D axially symmetric harmonic oscillator read in terms of action-angle variables (for a derivation, see Appendix A)

$$\rho^2=\frac{\omega_0}{\omega_\rho}(2j_\rho+|m|-2\sqrt{j_\rho(j_\rho+|m|)}\cos 2\theta_\rho), \qquad (9a)$$

$$z^2=\frac{2j_z\omega_0}{\omega_z}\sin^2\theta_z, \qquad (9b)$$

and $p_\rho=\dot{\rho}/\omega_0,p_z=\dot{z}/\omega_0$. Here, $j_z=J_z/\hbar$ and $j_\rho=J_\rho/\hbar$. If $\omega_z>\omega_\rho$ one averages over the angle $\theta_z=\omega_z t$. As a result, the motion effectively decouples into an unperturbed motion in the z coordinate governed by the potential $(\omega_z/\omega_0)^2z^2/2$ and into the relative motion in the ρ coordinate governed by the effective potential (see Appendix B)

$$V_{\mathrm{eff}}(\rho,j_z)=\frac{1}{2}\left(\frac{\omega_\rho}{\omega_0}\right)^2\rho^2+\frac{m^2}{2\rho^2}+\frac{\lambda}{\pi\rho}K\left(-2\frac{\omega_0}{\omega_z}\frac{j_z}{\rho^2}\right), \qquad (10)$$

where $K(x)$ is the first elliptic integral. Hence, the effective Hamiltonian reads

$$\epsilon=\frac{p_\rho^2}{2}+V_{\mathrm{eff}}-\frac{\omega_L}{\omega_0}m+\frac{\omega_z}{\omega_0}j_z. \qquad (11)$$

Applying a similar procedure as in the 2D case, we calculate the action integral numerically. The momentum p_ρ is determined from Eq. (11) and the turning points $\rho_{\mathrm{min}},\rho_{\mathrm{max}}$ are as usual the (positive) roots of the equation $p_\rho(\rho)=0$. Finally, the WKB-quantization conditions

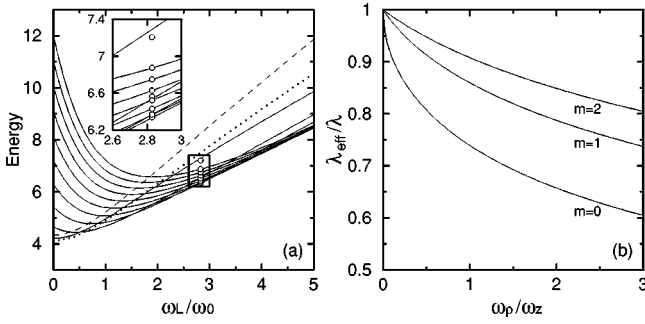$$I_\rho(\epsilon)=\hbar\left(n_\rho+\frac{1}{2}\right), \quad j_z=n_z+\frac{1}{2},$$

FIG. 3. (a) The comparison between energy levels (in units $\hbar\omega_0$) of the axially symmetric 3D quantum dot with $\omega_z/\omega_0=3$ and $\lambda=3$ for $n_\rho=n_z=0$ and $m=0,\ldots,9$ obtained using the RRM (full lines) and exact results for the spherical case (circles). The inset shows a good agreement between the RRM and the exact results. The dashed and dotted lines display the energy level with $m=0$ for the 2D and 3D cases with λ_{eff} at $\omega_0/\omega_z=0$ and $1/3$, respectively. (b) The dependence of the effective strength of the Coulomb interaction λ_{eff}/λ on the ratio ω_ρ/ω_z.

$$n_\rho,n_z=0,1,2,\ldots, \quad m=0,\pm 1,\pm 2,\ldots, \qquad (12)$$

determine the energy levels.

C. The effective charge

Comparing the exact and the RRM results for eigenenergies for the spherical case $\omega_z/\omega_\rho=1$ we found good agreement even for large values of the magnetic field [Fig. 3(a)] although RRM is expected to work best for $\omega_\rho/\omega_z<1$. Without magnetic field we have $\omega_\rho/\omega_z=1/3$ that means that the motion in z and ρ approximately decouples justifying the widely used 2D approximation. This is also reflected in the small difference between 2D and 3D results [compare Fig. 2(b) with Fig. 3(a) at $\omega_L=0$]. Turning on the magnetic field increases the coupling of the dynamics in ρ and z that allows the two electrons eventually to access the full 3D space. As a consequence, the electrons can avoid each other more effectively and the Coulomb interaction has a smaller effect on the 3D spectrum than on the 2D spectrum that is most clearly visible for the $m=0$ energies, see Fig. 3(a).

We can understand this effect quantitatively by averaging the elliptic integral in Eq. (10) over the unperturbed ($\lambda=0$) motion in ρ. It gives rise to an effective charge in the Coulomb interaction $V_C\approx\lambda_{eff}/2\rho$, where

$$\lambda_{eff}=\frac{2\lambda}{\pi^2}\int_0^\pi K\left(-\frac{\omega_\rho/\omega_z}{1+|m|-\sqrt{1+2|m|}\cos 2\theta_\rho}\right)d\theta_\rho \qquad (13)$$

for $n_\rho=n_z=0$ ($j_\rho=j_z=1/2$). The 3D energy quantized with this effective charge for the repulsion is close to the full interaction [dotted line in Fig. 3(a)].

The effective charge λ_{eff}/λ as a function of ω_ρ/ω_z for different m is shown in Fig. 3(b). The maximum repulsion at $\omega_\rho/\omega_z=0$ corresponds with $\omega_z\to\infty$ to the 2D case. The 3D case without magnetic field starts for our parameters $\omega_\rho/\omega_z=1/3$ at some value $\lambda_{eff}/\lambda<1$ that decreases further for increasing ω_ρ/ω_z, i.e., increasing magnetic field. This

explains quantitatively through the effective charge the difference of the effect of a magnetic field on a quantum spectrum in 2D and 3D cases. However, this difference becomes weaker for larger m as it is seen in Fig. 3(b). The effective charge clearly demonstrates that the Coulomb interaction is stronger, especially for small m, in the 2D case compared to the 3D case. This simply understandable classical finding clarifies numerical quantum-mechanical results obtained for the 2D and 3D cases of many-electron QD's.[23]

IV. OBSERVABLE CONSEQUENCES OF THE THIRD DIMENSION IN QUASI-2D QUANTUM DOTS

A. The first singlet-triplet transition in the two-electron QD

The ground-state energy of a QD as a function of the magnetic field can be probed very elegantly by single electron capacitance spectroscopy[11] or by single electron tunnelling spectroscopy.[10] Applying a gate voltage to the contacts brings the electrochemical potential of the contacts in resonance with the energy $\mu(N,B)$ necessary to add the Nth electron that tunnels through the barrier into the dot. The chemical potential of the dot is given by the ground-state energy of the dot with N and $N-1$ electrons (see,e.g., Ref. 10),

$$\mu(N,B)=E(N,B)-E(N-1,B). \qquad (14)$$

Here, $E(N,B)$ denotes the total energy of the QD with N electrons under a magnetic field of strength B. Presently, we are concerned with $\mu(1,B)$ and $\mu(2,B)$ only. The first is simply the harmonic-oscillator energy for a single electron in the dot, $\mu(1,B)=E(1,B)$. The latter can be split into contributions from the relative and center-of-mass motion E_{CM}, where $E_{CM}=E(1,B)$. The most direct probe of electron correlation in the quantum dot is the *difference* of the chemical potentials that takes the form

$$\Delta\mu_{21}\equiv\mu(2,B)-\mu(1,B)=\hbar\omega_0\epsilon-E(1,B), \qquad (15)$$

where ϵ is the relative energy of Eq. (2) and $E(1,B)=\hbar\omega_\rho+\hbar\omega_z/2$.

In a number of papers (e.g., Refs. 10,11,13,17) $\mu(1,B)$ has been used to estimate the confining frequency $\hbar\omega_0$ in a two-dimensional model of the QD. Indeed, with $\hbar\omega_0=5.4$ meV ($\hbar\omega_z=0$) one obtains a very satisfactory fit to $\mu(1,B)$. However, with this $\hbar\omega_0$, neither $\Delta\mu_{21}$ (which is by almost a factor 2 too large) nor the value for B, where the first singlet-triplet transition occurs, is reproduced correctly as is obvious from Fig. 4(a). It has been argued that for increasing magnetic field $\mu(N,B)$ might not follow the behavior modeled with a pure QD with constant confining frequency, see Refs. 10,17, and Ref. 11 in Ref. 13. Hence, we believe it is more realistic to extract $\hbar\omega_0$ from the difference of the chemical potentials $\mu(2,0)-\mu(1,0)$ at zero magnetic field. This has been done in Fig. 4(a) and leads with $\hbar\omega_0=2.3$ meV ($\lambda=3.32$) to the first singlet-triplet splitting at $B=1.02$ T. This value differs from the experimental value of $B\approx1.5$ T only by about 30% in contrast to the difference of more than a factor 2 with $\hbar\omega_0=5.4$ meV (dashed line).
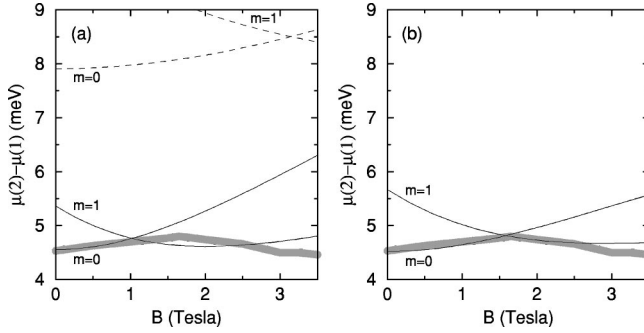
FIG. 4. Difference $\Delta\mu$ of electrochemical potentials, Eq. (15), from the experiment[11] (shaded curve). (a) shows the theoretical $\Delta\mu_{21}$ from a 2D quantum dot model with $\hbar\omega_0 = 5.4$ meV (dashed) and $\hbar\omega_0 = 2.3$ meV (solid). (b) shows $\Delta\mu_{21}$ from a 3D model with $\hbar\omega_0 = 2.6$ meV and $\omega_z/\omega_0 = 2.4$ (solid).

The discrepancy of 30% vanishes if one proceeds to a 3D description of the QD. In this case $\hbar\omega_0 = 2.6$ meV ($\lambda = 3.12$) is needed to match $\mu(2,0) - \mu(1,0)$, only slightly different from the 2D case, but the first singlet-triplet transition occurs now at $B = 1.59$ T [see Fig. 4(b)]. If one includes the contribution from the Zeeman energy (with $g^* = -0.44$) this value reduces to $B = 1.52$ T in a good agreement with the experiment. Of course, this agreement is achieved by tuning a second parameter, available in the 3D case, namely, $\omega_z/\omega_0 = 2.4$, i.e., the ratio of vertical to lateral confinement. On the other hand, a rough estimate assuming $\omega_z/\omega_0 \sim d_0/d_z$ (see, for example, Ref. 6) reveals with the experimental value $d_z = 175$ Å, a lateral size of $d_0 \approx 420$ Å that is the correct order of magnitude although the exact lateral extension in the experiment is not known.[11]

The analysis shows that in contrast to a 2D description the 3D description provides a way to describe the energy spectrum for small B, the value of the magnetic field for the first singlet-triplet transition, and the ratio of lateral to vertical extension of the dot consistently.

B. Magnetic moment and susceptibility

The singlet-triplet transitions in the ground-state energy appear as discontinuities in the magnetic properties of the dot. For temperature $T = 0$ the magnetic moment and the magnetic susceptibility are defined by $\mu_{\mathrm{mag}} = -\partial E_{\mathrm{gr}}/\partial B$ and $\chi = \partial\mu_{\mathrm{mag}}/\partial B$, respectively. We find that the resulting spikes shift when going from the 2D quantum dot to the 3D case as shown in Fig. 5. For the parameters used in the results of Figs. 2 and 3 the shift in the magnetic field can be calculated from the relation $\Delta B \approx 3.47\Delta x$ T where $x = \omega_L/\omega_0$. For example, in the region $1.25 < x < 1.5$ we obtain that the spike in the magnetic moment should occur in the 3D case at the magnetic field that is by $\Delta B \approx 0.8$ T higher than the one expected for the 2D case. The increase/decrease of the confining frequency in the third dimension at fixed value of the lateral confinement will decrease/increase the difference between the 2D and 3D predictions for spikes of the magnetic moment and magnetization.
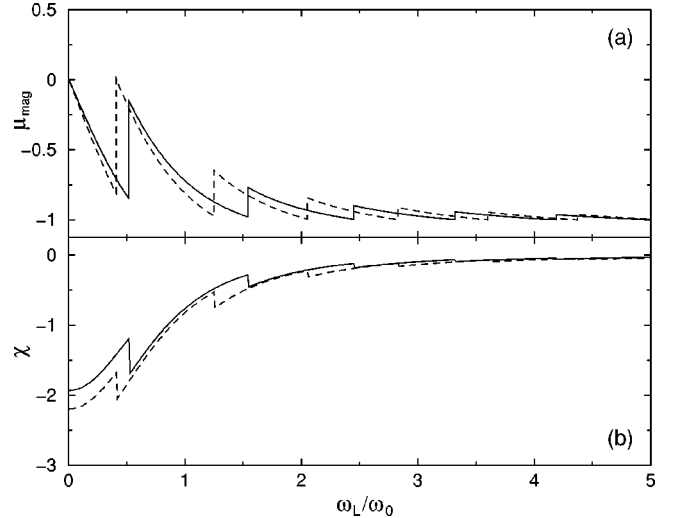

FIG. 5. Magnetic moments μ_{mag} (a) in the units of effective Bohr magneton $\mu_B^* = (m_e/m^*)\,\mu_B$ and the magnetic susceptibility χ (b) for the 2D (dashed lines) and 3D (full lines) cases as a function of the magnetic-field strength (in ω_L/ω_0-units). We use the same parameters as in Figs. 2 and 3.

V. SUMMARY

By relaxing the restriction of two dimensions for a quantum dot and working in the physical three-dimensional space we have investigated physical examples of nonintegrable systems close to integrability. Using the classical RRM we could effectively reduce the nonintegrable problem of two electrons in the parabolic potential under the perpendicular magnetic field to an integrable case. Under these circumstances the WKB-approach provides a simple and transparent way to calculate the spectrum of the 3D two-electron QD and produces reliable results even for the ground state.

We have found that at *specific* values of the magnetic field $\omega_L^* = \sqrt{\omega_z^2 - \omega_0^2}$ an axially symmetric QD exhibits spherical symmetry. At these values its dynamics becomes completely separable with three integrals of motion and three corresponding quantum numbers, since the electron-electron interaction does not break spherical symmetry.

We have shown how the confinement in the z direction, neglected in the 2D description of quantum dots, does have an influence on the spectrum. In fact, the vertical confinement reduces the Coulomb repulsion between electrons. Including the third dimension a consistent description of the experimental data[11] becomes possible. Finally, by changing the confining frequency in the z direction only slightly one can increase or decrease the magnetic moment and the susceptibility, i.e., one can control the magnetic properties of the two-electron quantum dot.

APPENDIX A

We briefly derive the action-angle variables for the axially symmetric 3D harmonic oscillator. Straightforward but tedious to calculate these expressions cannot be found in textbooks that contain only the general transformation formulas, see, e.g., Ref. 20.

The Hamiltonian can be written in the form

$$\epsilon_0 = \epsilon_\rho + \epsilon_z, \tag{A1}$$

where

$$\epsilon_\rho = \frac{p_\rho^2}{2} + \frac{m^2}{2\rho^2} + \frac{\tilde{\omega}_\rho^2 \rho^2}{2}, \quad \epsilon_z = \frac{p_z^2}{2} + \frac{\tilde{\omega}_z^2 z^2}{2}, \tag{A2}$$

and $\tilde{\omega}_\rho = \omega_\rho/\omega_0, \tilde{\omega}_z = \omega_z/\omega_0$.

The momenta as functions of the corresponding coordinates depend on the energies of the oscillator modes

$$p_\rho = \pm \sqrt{2\epsilon_\rho - \tilde{\omega}_\rho^2 \rho^2 - m^2/\rho^2},$$

$$p_z = \pm \sqrt{2\epsilon_z - \tilde{\omega}_z^2 z^2} \tag{A3}$$

and the classical turning points

$$\rho_{\min,\max} = \frac{1}{\tilde{\omega}_\rho}(\epsilon_\rho \mp \sqrt{\epsilon_\rho^2 - \tilde{\omega}_\rho^2 m^2})^{1/2},$$

$$z_{\min,\max} = \mp \frac{1}{\tilde{\omega}_z}\sqrt{2\epsilon_z} \tag{A4}$$

are the roots of equations $p_\rho(\rho)=0, p_z(z)=0$.

The corresponding action integrals

$$j_\rho = \frac{1}{2\pi} \oint p_\rho d\rho = \frac{1}{\pi}\int_{\rho_{\min}}^{\rho_{\max}} \sqrt{2\epsilon_\rho - \tilde{\omega}_\rho^2 \rho^2 - m^2/\rho^2}\, d\rho,$$

$$j_z = \frac{1}{2\pi} \oint p_z dz = \frac{2}{\pi}\int_0^{z_{\max}} \sqrt{2\epsilon_z - \tilde{\omega}_z^2 z^2}\, dz \tag{A5}$$

can be solved analytically

$$j_\rho = \frac{1}{2}\left(\frac{\epsilon_\rho}{\tilde{\omega}_\rho} - |m|\right), \quad j_z = \frac{\epsilon_z}{\tilde{\omega}_z} \tag{A6}$$

and the energies of these two oscillatory modes are expressed in terms of the corresponding action variables

$$\epsilon_\rho = \tilde{\omega}_\rho(2j_\rho + |m|), \quad \epsilon_z = \tilde{\omega}_z j_z. \tag{A7}$$

In order to express the ρ, z coordinates in terms of the action-angle variables, the equations of motion

$$\frac{d\rho}{d\tau} = p_\rho, \quad \frac{dz}{d\tau} = p_z \tag{A8}$$

must be integrated. The scaled time variable $\tau = \omega_0 t$ is introduced in order to keep the dimensionless form of equations of motion. Therefore

$$\int_{\rho_0}^{\rho} \frac{d\rho}{\sqrt{2\epsilon_\rho - \tilde{\omega}_\rho^2 \rho^2 - m^2/\rho^2}} = \tau,$$

$$\int_{z_0}^{z} \frac{dz}{\sqrt{2\epsilon_z - \tilde{\omega}_z^2 z^2}} = \tau. \tag{A9}$$

Using initial values $\rho_0 = \rho_{\min}, z_0 = 0$, we obtain

$$\arcsin\left(\frac{\tilde{\omega}_\rho^2 \rho^2 - \epsilon_\rho}{\sqrt{\epsilon_\rho^2 - \tilde{\omega}_\rho^2 m^2}}\right) + \frac{\pi}{2} = 2\omega_\rho t,$$

$$\arcsin\frac{\tilde{\omega}_z z}{\sqrt{2\epsilon_z}} = \omega_z t, \tag{A10}$$

or inverting

$$\rho^2 = \frac{1}{\tilde{\omega}_\rho^2}(\epsilon_\rho - \sqrt{\epsilon_\rho^2 - \tilde{\omega}_\rho^2 m^2}\cos 2\omega_\rho t),$$

$$z = \frac{\sqrt{2\epsilon_z}}{\tilde{\omega}_z}\sin \omega_z t. \tag{A11}$$

Finally, using expressions (A7) we have

$$\rho^2 = \frac{1}{\tilde{\omega}_\rho}(2j_\rho + |m| - 2\sqrt{j_\rho(j_\rho + |m|)}\cos 2\theta_\rho), \tag{A12}$$

$$z = \sqrt{\frac{2j_z}{\tilde{\omega}_z}}\sin \theta_z, \tag{A13}$$

where $\theta_\rho = \omega_\rho t, \ \theta_z = \omega_z t$.

APPENDIX B

If $\omega_z > \omega_\rho$ we average the Hamiltonian for the relative motion, Eq. (2), over the angle θ_z. Therefore, it is enough to express only z variables in terms of the corresponding action-angle variables

$$\epsilon = \epsilon_\rho(p_\rho, \rho) + \tilde{\omega}_z j_z - \frac{\omega_L}{\omega_0}m + v_c, \tag{B1}$$

where the energy ϵ_ρ is given by Eq. (A2) and

$$v_c = \frac{\lambda}{2\rho}\left(1 + \frac{2j_z}{\tilde{\omega}_z \rho^2}\sin^2\theta_z\right)^{-1/2}. \tag{B2}$$

Since the Coulomb term is the only one that depends on the angle θ_z, the procedure reduces to evaluation of the effective Coulomb interaction

$$v_c^{\text{eff}} = \frac{1}{2\pi}\int_0^{2\pi} v_c(\rho, j_z, \theta_z)\, d\theta_z = \frac{\lambda}{\pi\rho}K\left(-\frac{2j_z}{\tilde{\omega}_z \rho^2}\right), \tag{B3}$$

where K is the first elliptic integral. Thus, the full effective potential Eq. (10) depends only on the ρ coordinate.

[1] R. Turton, *The Quantum Dot. A Journey into Future Microelectronics* (Oxford University Press, New York, 1995).

[2] D. Bimberg, M. Grundmann, and N. N. Ledentsov, *Quantum Dot Heterostructures* (Wiley, New York, 1998).

[3] T. Chakraborty, *Quantum Dots* (Elsevier, Amsterdam, 1999).

[4] L.P. Kouwenhoven, D.G. Austing, and T. Tarucha, Rep. Prog. Phys. **64**, 701 (2001).

[5] M. Macucci, K. Hess, and G.J. Iafrate, Phys. Rev. B **48**, 17 354 (1993); J. Appl. Phys. **77**, 3267 (1995); A. Wojs and P. Hawrylak, Phys. Rev. B **53**, 10 841 (1996).

[6] W.D. Heiss and R.G. Nazmitdinov, Phys. Lett. A **222**, 309 (1996); Phys. Rev. B **55**, 16 310 (1997); Pis'ma Zh. Eksp. Tekh. Fiz **68**, 870 (1998) [JETP Lett. **68**, 915 (1998)].

[7] Y. Alhassid, Rev. Mod. Phys. **72**, 895 (2000).

[8] P.A. Maksym, H. Imamura, G.P. Mallon, and H. Aoki, J. Phys.: Condens. Matter **12**, R299 (2000).

[9] Bo Su, V.J. Goldman, and J.E. Cunningham, Phys. Rev. B **46**, 7644 (1992).

[10] T. Schmidt, M. Tewordt, R.H. Blick, R.J. Haug, D. Pfannkuche, K.v. Klitzing, A. Förster, and H. Lüth, Phys. Rev. B **51**, 5570 (1995).

[11] R.C. Ashoori, H.L. Stormer, J.S. Weiner, L.N. Pfeiffer, K.W. Baldwin, and K.W. West, Phys. Rev. Lett. **71**, 613 (1993).

[12] R.C. Ashoori, Nature (London) **379**, 413 (1996).

[13] L.P. Kouwenhoven, T.H. Oosterkamp, M.W.S. Danoesastro, M. Eto, D.G. Austig, T. Honda, and S. Tarucha, Science **278**, 1788 (1997).

[14] U. Merkt, J. Huser, and M. Wagner, Phys. Rev. B **43**, 7320 (1991); M. Wagner, U. Merkt, and A.V. Chaplik, *ibid.* **45**, 1951 (1992).

[15] M. Dineykhan and R.G. Nazmitdinov, Phys. Rev. B **55**, 13 707 (1997); J. Phys.: Condens. Matter **11**, L83 (1999).

[16] P. Hawrylak, Phys. Rev. Lett. **71**, 3347 (1993).

[17] J.J. Palacios, L. Martin-Moreno, G. Chiappe, E. Louis, and C. Tejedor, Phys. Rev. B **50**, 5760 (1994).

[18] V. Fock, Z. Phys. **47**, 446 (1928); C.G. Darwin, Proc. Cambridge Philos. Soc. **27**, 86 (1930).

[19] B. Meurer, D. Heitmann, and K. Ploog, Phys. Rev. B **48**, 11 488 (1993).

[20] A. J. Lichtenberg and M. A. Lieberman, *Regular and Chaotic Dynamics*, 2nd ed. (Springer-Verlag, New York, 1992).

[21] A.V. Madhav and T. Chakraborty, Phys. Rev. B **49**, 8163 (1994).

[22] A. Wojs, P. Hawrylak, S. Fafard, and L. Jacak, Phys. Rev. B **54**, 5604 (1996).

[23] N.A. Bruce and P.A. Maksym, Phys. Rev. B **61**, 4718 (2000).